Engineering Structures 303 (2024) 117570

Contents lists available at ScienceDirect

Engineering Structures

journal homepage: www.elsevier.com/locate/engstruct

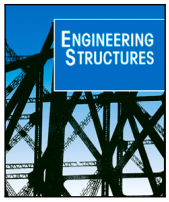

On using autoencoders with non-standardized time series data for damage localization

Niklas Römgens *, Abderrahim Abbassi, Clemens Jonscher, Tanja Grießmann, Raimund Rolfes

Leibniz University Hannover, Institute of Structural Analysis, Appelstraße 9A, 30167 Hanover, Germany

ARTICLE INFO

Keywords:
Autoencoder
PCA
Unsupervised damage localization
Data-driven model
Structural health monitoring

ABSTRACT

In this paper, an autoencoder trained with non-standardized time series data and evaluated using covariance-based residuals for generally applicable unsupervised damage localization is investigated. Raw acceleration time series are used as the inputs for the autoencoder to give both these features: no loss of information and exploitation of the full potential of the neural network. When it comes to output-only and unsupervised structural health monitoring (SHM), data-driven models struggle to localize the positions of damage adequately or only work well in a small range of applications. Regarding neural networks, expertise is needed for the neural network dimensioning and understanding of structural dynamics, which increases the difficulty of the task. In order to simplify the process, an automated solution is provided to perform the neural architecture search, and principal component analysis (PCA) is used to find a good choice for the bottleneck dimension. As an extension of the model, the residuals between the original and reconstructed time series are evaluated using the covariance between each input signal and each residual time series, which results in improved indicators for damage localization. We demonstrate the efficiency of the proposed schemes for damage analysis in a series of simulations using a three-mass swinger, in which the autoencoder can localize the damage using varying excitation locations. The covariances' evaluation indicates that they are more potent than using the reconstruction error. Finally, experimental validation is conducted using vibration test data from a lattice tower called Leibniz University Structure for Monitoring (LUMO) under ambient excitation. For each damage pattern, high sensitivity towards local stiffness is achieved. Additionally, the damage position indicators exhibit a clear decreasing trend as the distance from the damage increases. The autoencoders presented here with non-standardized time series and covariance-based evaluation of residuals lead to increased robustness and sensitivity regarding damage localization.

1. Introduction

Wind turbines are exposed to high loads arising from wind and waves. Additionally, different factors such as material aging, environmental corrosion, or poor construction quality need to be considered [1]. To guarantee the safety of structures, structural health monitoring (SHM) is a necessity. SHM encompasses the systematic observation and analysis of a system over time using periodically sampled response measurements to monitor changes. When these changes are associated with damage, the goals can be to (i) detect, (ii) localize, (iii) classify, and (iv) quantify the damage, while (v) predicting the remaining life of the structure [2,3]. The core principle of vibration-based SHM is the assumption that potential damage alters the dynamic properties of a structure. Consequently, it is obviously useful from a physics-based perspective to track changes in the modal features, such as mode shapes or mode shape curvatures of the structures. These features hold potential for damage localization [4,5], but require a high spatial [6] and temporal resolution [7], which is inefficient both in terms of application and economy. FE model updating is part of the physics-based models, in which damage-induced variations in the mechanical properties cause detectable changes in the structural dynamic behavior [8,9]. The authors introduced the application of a parameterized damage distribution function [10,11] and extended it in [12]. Model updating allows for relatively precise damage localization using modal parameters, which can advantageously be interpreted physically. For this purpose, an FE model with some unknown quantities, e.g., contact stiffnesses, has to be set up. Environmental and operational conditions (EOCs) can only be represented in the model at considerable additional expense. In addition, a general weakness of the model updating approach lies in the modeling of the damage.

In contrast, data-driven models do not need any physical assumptions. Hence, a major focus of SHM studies in recent years has been

* Corresponding author.
E-mail address: n.roemgens@isd.uni-hannover.de (N. Römgens).

https://doi.org/10.1016/j.engstruct.2024.117570
Received 21 August 2023; Received in revised form 14 December 2023; Accepted 23 January 2024
Available online 28 January 2024

devoted to developing unsupervised vibration-based monitoring techniques and using data-driven models, in which no physical insight is given to the model [13]. This work focuses on addressing the specific challenge of localizing damage in output-only and unsupervised data-driven vibration-based SHM and builds upon the existing contributions made by various authors. Mosavi et al. [14] applied the Mahalanobis distance to identify vector autoregressive (VAR) parameters for damage localization. Chesné and Deraemaeker [15] discussed the use of transmissibility functions for damage localization. Various factors, such as the selection of frequency bands, environmental effects, and reliance on the location of the force, hinder the practicality of damage localization using these functions. Wernitz [13] used linear quadratic estimation theory to localize the induced damage in a girder mast exposed to natural sources of excitation and uncertainty. The efficacy of the proposed data normalization strategies could not be proven. Hofmeister [16] presented a method for damage localization based on finite impulse response filters with multiple inputs and applied directly to measurement data. The localization accuracy and robustness using the data-driven approach were not satisfactory. Alves and Cury [17] focused on the extraction of features using domain association (time, frequency, and quefrency domains) and an unsupervised feature selection technique, which have been successfully applied to real-world monitoring situations. Due to their strong capacity for generalization, the application of autoencoders in vibration-based SHM has increased over the last few years. Anaissi et al. [18] used the energy levels of standardized time series data as the inputs of an autoencoder to monitor the health state of a bridge and a three-storey building. No information was provided about the size of the bottleneck dimension, which is the smallest dimension of the autoencoder. Ma et al. [19] used standardized acceleration signals as the inputs to a C-VAE (Convolutional-Variational Autoencoder) to monitor a bridge with a moving train. Zhang et al. [20] presented a method using wavelet packet energy and C-VAE for damage localization in a subway tunnel. Römgens et al. [21] showed that autoencoders with time series are suitable for damage localization under ambient conditions. The dimensioning of the neural network was not automated and only selected short response time series were used. In the publications above, it is expected for structural systems under investigation that measurement channels will not align with the estimated values in case of local instances of damage. The damage positions can be narrowed down to adjacent channels by evaluating errors. A particular challenge is to deal with the transfer from simulations to systems under ambient excitation with varying EOCs. Usually, the methods developed are not generally applicable and only have a small range of applications. Another essential step is the dimensioning of the neural network, which is often disregarded but plays an important role.

The aim of this paper is to achieve more robustness regarding excitation type and position for damage localization by using a traditional autoencoder. Greater robustness is also desired with regard to the underlying environmental conditions. In summary, the contributions of this paper are threefold: (i) Time series data are used as the inputs of an autoencoder for unsupervised damage localization. Due to its efficiency regarding implementation and computational cost, no convolutional layers or specific probabilistic distribution are chosen for the neural network. (ii) The inputs are non-standardized, and an automated solution is provided to perform the neural architecture search, which makes this approach generally applicable. An efficient way to determine the bottleneck dimension is provided by principal component analysis (PCA). (iii) A new damage-sensitive feature for damage localization is investigated in which the covariance of the residuals and the input signals are evaluated.

The structure of the paper is as follows. The fundamental theory of autoencoders is reviewed in Section 2. The data generation for the simulation model and the results obtained are presented in Section 3. The experimental setup and the results of the experimental validation are explained and discussed in Section 4.

2. Theoretical background

In this paper, the dynamic properties of the structures under investigation are learned using the autoencoder. Hence, the generally known theory of autoencoders and the learning process are necessary for explanation, to which Section 2.1 is dedicated. In Section 2.2, the inputs of the autoencoder are discussed in more detail and also how the architecture of the neural network can be determined for this purpose. An effective approach to analyzing the residuals of the autoencoder is presented in the last section, and is seemingly very practical in evaluations with neural networks [21].

2.1. Autoencoder

As special types of artificial neural networks, autoencoders are employed to acquire proficient encodings of unlabeled data. A typical application is the use of autoencoders as anomaly detectors [22–24] or to reduce the dimensionality of the data [25,26].

In practice, a network of artificial neurons is trained to reconstruct the original input matrix X. Due to the autoencoders' network structure, the model is aimed to find a lower-dimensional representation of the input data while retaining the most important information. The first component of an autoencoder network, known as the *encoder*, plays a crucial role in compressing the input information from its high-dimensional input space into a lower-dimensional latent space (bottleneck dimension). This compression is achieved by extracting and encoding salient features from the input data, effectively reducing its dimensionality. Subsequently, the second component, referred to as the *decoder*, focuses on reconstructing the input signals from the compressed representation obtained by the encoder. By leveraging the bottleneck dimension, the decoder employs various reconstruction techniques to generate the outputs that closely resembles the original inputs. The differences between the original data y and the reconstructed data $\hat{y}$ can be summarized as a performance index that evaluates the loss of information resulting from dimensional reduction. To predict the error of the neural network, the mean squared error function J is commonly employed [27]

$$J(W,b) = \frac{1}{n}\sum_{i=1}^{n}(\hat{y}^{(i)} - y^{(i)})^2. \tag{1}$$

The so-called loss function J is used to modify the weightings for each iteration k

$$W_{ji,k+1}^{(l)} = W_{ji,k}^{(l)} - \lambda\frac{\partial J}{\partial W_{ji}^{(l)}}. \tag{2}$$

The weightings serve as the connections between adjacent layers and are summarized in a weight matrix W_{ji}. The network parameters are updated with regard to the calculated loss using the learning rate λ, which is a hyperparameter and needs to be tuned. With increasing number of training epochs, the performance of the model improves as the parameters of the model are optimized. An algorithm for first-order gradient-based optimization of stochastic objective functions called ADAM is best suited for this [28], which is well known in the field of deep learning.

2.2. Time series data as inputs

Various information, such as modal parameters [29], spectra [30] and standardized time series [19], can be used as the inputs for an autoencoder. For the approach presented, non-standardized time series are used as input variables, because the amplitude relationships of the time series are not changed by standardization or normalization and also to exploit the full potential of the neural network. In data acquisition, the time series data are acquired continuously at a sampling rate of f_s. Each time series is divided into a defined number of sequences;

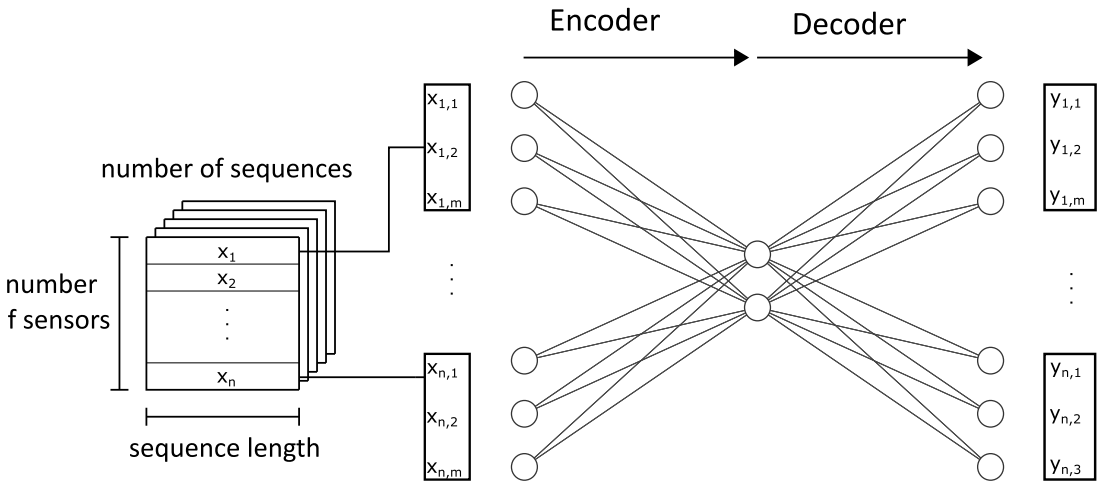

Fig. 1. Splitting of time series using a defined sequence length (left) and how these values are fed to the autoencoder (right).

the length of the sequences l can be estimated according to [19] to acquire the main dynamic response

$$l \geq 2\frac{f_s}{f_1}, \tag{3}$$

where f_1 is the fundamental frequency of the response. For a longer sequence length and a correspondingly larger input dimension, the autoencoder can require a more complex architecture with additional layers or larger hidden representations, resulting in extra computational cost. As an advantage, longer sequences enable the autoencoder to capture and represent longer-term dependencies or patterns in the input data. It is important to note that when using the autoencoder, frequencies below the fundamental frequency can also be reconstructed well, as the model learns mainly to map the input signals to the outputs as well as possible.

Considering the sequence length, the autoencoder can be appropriately dimensioned to handle time series data as illustrated in Fig. 1. An overview of the data transfer process and the simplified structure of the autoencoder is provided, emphasizing its ability to accurately reconstruct input values x. By adjusting the weightings, represented by the connections between the neurons, the target vectors y should be approximated as accurately as possible. The number of neurons in the input and output layers corresponds to the dimension of the input vectors x.

Since autoencoders are used in many different areas and are also developing their potential in various applications [31], there are many ways to determine the bottleneck dimension, e.g., an approach based on mutual information [32]. However, a unique approach has been chosen for the application with time series. Due to its simplicity and low computational time, the PCA is used instead of the autoencoder's repeated training across various bottleneck dimensions to approximate the reconstruction of the signals. This allows us to estimate the significance of each additional principal component. In general, the differences between the target y and the output vectors $\hat{y}$ decrease in the time domain as the number of principal components in the PCA increases. The evaluation of the differences in the time domain proves to be impractical in many cases, leading to an overemphasis on noise or irrelevant features. Hence, the predicted values and target values are further transformed into the frequency domain using spectral density estimation based on Welch's method (as carried out in [33]) to evaluate the differences for varying numbers of principal components l.

$$p_l = |\hat{G}(y) - \hat{G}(\hat{y}_l)| \tag{4}$$

A good choice for the number of principal components has been made once the model no longer continues to improve

$$p_l \approx p_{l+1} \approx p_{l+2} \approx p_{l+3}. \tag{5}$$

With the determination of the sequence length and the bottleneck dimension, the neural network's configuration can thus be defined and the hyperparameters can be adjusted using Bayesian optimization.

2.3. Damage localization method

The autoencoder's ability to detect anomalies, such as structural change or damage, can be used for damage analysis. To accomplish this, the autoencoder should, after training, be able to accurately reconstruct time series data from a healthy state, which for the difference between the target values y_k and the estimated values $\hat{y}_k$ for each discrete time step k can be calculated

$$e_k = y_k - \hat{y}_k. \tag{6}$$

The differences can be determined individually for each time series i

$$e_{i,k} = y_{i,k} - \hat{y}_{i,k}. \tag{7}$$

A typical approach is to evaluate its mean or covariance [13]. The underlying assumption is that the channel closest to the damage exhibits the greatest difference compared to the healthy reference. The mean absolute error $E_{i,abs}$ can be calculated for each sensor and is known as the reconstruction error of the network's output

$$E_{i,abs} = \frac{1}{m}\sum_{k=1}^{m}|e_{i,k}|. \tag{8}$$

For additional consideration of the inputs, the absolute covariance of the input signals x_j and the estimation errors e_i are calculated and divided by the number of time series n, namely the residual covariance $E_{i,cov}$

$$E_{i,cov} = \frac{1}{n}\sum_{j=1}^{n}|cov(x_j, e_i)|. \tag{9}$$

The idea is based on the fact that the autoencoder maps the essential structural properties; hence, input signals corresponding to a different state are not well reconstructed. The estimation errors consist of deterministic components not absorbed by the model, which the residual covariance quantifies. Since each estimated output signal is reconstructed using a sum of all input signals, the covariance from each input time series is averaged with the error time series of the output. If a feature (e.g., time series) of the autoencoder is particularly dominant, the averaging can reduce these effects. The covariances are used to quantify the contributions of individual features to the prediction or outcome of a machine learning model, improving the interpretability and transparency of the model.

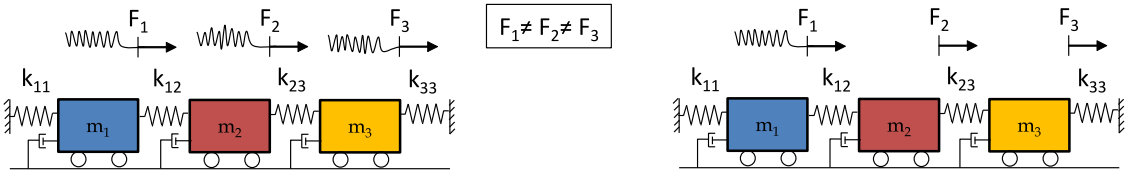

Fig. 2. Illustration of the simulation model being excited at all masses (left), and only at mass m_1 (right).

Table 1
Modal parameters of the system from simulated data for healthy and damaged states.

Name	Position	f1	f2	f3
Healthy	–	12.18 Hz	22.51 Hz	29.41 Hz
(a)	k11	**11.94 Hz**	22.24 Hz	29.29 Hz
(b)	k12	**12.14 Hz**	22.17 Hz	28.79 Hz
(c)	k23	**12.11 Hz**	22.21 Hz	28.82 Hz
(d)	k33	**11.91 Hz**	22.19 Hz	29.32 Hz

3. Simulation study

To show the applicability of autoencoders with time series data for damage localization, a 3DOF system is investigated. Mainly to demonstrate robustness regarding varying damage positions, the excitation at all masses and at one mass will be simulated and presented in the first section (Section 3.1). For the evaluation of the models, four different damage positions are examined simultaneously in Section 3.2. By averaging the estimation error, a damage indicator can be derived, which is compared to a potentially more potent damage position indicator, as described in Section 2.3.

3.1. 3DOF system

A 3DOF system is represented in the form of the spring–mass chain depicted in Fig. 2. Each mass was chosen to be 1 kg and each stiffness 10 $\mathrm{kNm^{-1}}$. Proportional damping was defined by a damping rate of 0.01 for each of the three eigenmodes. In this way, the inputs and outputs of the model were repetitively simulated for a duration of 60,000 samples at a sampling frequency of 100 Hz (600 s). To this end, each mass was excited with Gaussian white noise, featuring a variance of 0.1 $\mathrm{N^2}$. Measurement noise taken from a Gaussian distribution with a variance of $5 \cdot 10^{-6}\mathrm{m^2/s^4}$ and was added to the input signals. The same stiffness matrix is used for generating validation data sets, only varying the Gaussian white noise (same variance). Damage was realized by reducing each stiffness individually by 10% as described in [33].

Further, a different excitation location was chosen using Gaussian white noise acting only on mass m_1 (see Fig. 2). Again, four different springs k_{11}, k_{12}, k_{23} and k_{33} are each sequentially weakened by 10%. Table 1 shows the resulting frequencies when the stiffness reduction is applied. The eigenfrequencies are estimated by solving the eigenvalue problem of the stiffness and mass matrix. Due to the small system size, all natural frequencies are considered, and accordingly, the fundamental frequency is $f1$. The sequence length l is determined using Eq. (3) and chosen to be 20 time steps (0.1 s long sequences) from each sensor

$$l = 20 \geq 2\frac{100}{11.91} = 16.79. \tag{10}$$

Since we are dealing with a lower limit in Eq. (3), the most significant natural frequency of $f1$ (11.91 Hz) is inserted into the formula. With three sensors, a sequence length of 20 results in an input quantity of 60.

For comparison, the reconstruction errors in the time domain and frequency domain are presented in Fig. 3. As described in Section 2.2, a suitable choice of the bottleneck dimension is determined using the PCA evaluating the frequency domain. A much more significant trend than evaluating the reconstruction error in the time domain can be observed. A higher number of principal components (see Fig. 4) indicates that the frequencies can be represented in the model. Only the noise components are reconstructed above a certain number of principal components so that only minor improvements in the frequency space can be achieved. The transformation to the frequency domain improves the interpretability and simplifies the selection. For the numbers 7 (mass m_1 excited) and 20 (all masses excited, cf. Fig. 3) principal components, only minor improvements in the reconstruction in the frequency domain could be achieved.

3.2. Results

Fig. 5 illustrates the reconstruction errors arising when evaluating 10 min data sets for validation and four different damage patterns, using a 10% reduction in the stiffness of springs k_{11}, k_{12}, k_{23}, and k_{33}. Different excitation positions are investigated using Gaussian distributed force at all masses and only at mass m_1. The bar colors correspond to the response time series relating to masses 1, 2, and 3, as seen in Fig. 2.

The data represent the local stiffness changes mainly linked to the induced damage instances using the autoencoder with non-standardized time series data. Notably, the reconstruction error of each signal can be successfully used as a damage position indicator. The reconstruction errors of the validation data sets imply that the time series of the healthy state can be reconstructed well using the autoencoder. Interestingly, the errors are very similar for the excitation at mass m_1 only, although the amplitudes of the original signals differ substantially. Due to the autoencoder's structure, the reconstruction signals are decoded from the bottleneck dimension, in which the information is compressed. This model property offers a significant advantage compared to, for example, autoregressive models [33] for the purpose of damage localization. A 10% reduction in the stiffness of spring k_{11} leads to a change in eigenfrequencies as described in Table 1. The change in the dynamic behavior results in a compromised reconstruction of the original time series. In particular, the time series for the mass m_1 is most poorly reconstructed, so the positions of the damage for both excitation positions can be deduced. The other damage cases can be analyzed in the same way by narrowing down the positions of damage to adjacent sensors.

For comparison, Fig. 6 illustrates the results using the residual covariance instead of the reconstruction error, evaluating the same time series errors as before. As described earlier, the residual covariance measures the remaining linear dependencies between the time series errors and the inputs of the model. Testing 10 min data sets from the structure in the healthy state, the original time series are well reconstructed, as already seen in Fig. 5. The reconstruction error of the data sets used for validation mainly consists of noise components, and averaging the linear dependencies between the input signals and the error time series by means of the covariance; very small values are

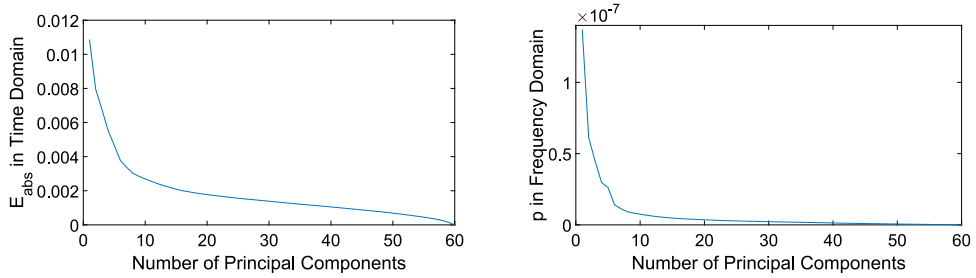

Fig. 3. Reconstruction error of PCA in the time domain (left) and frequency domain (right) for excitation at all masses.

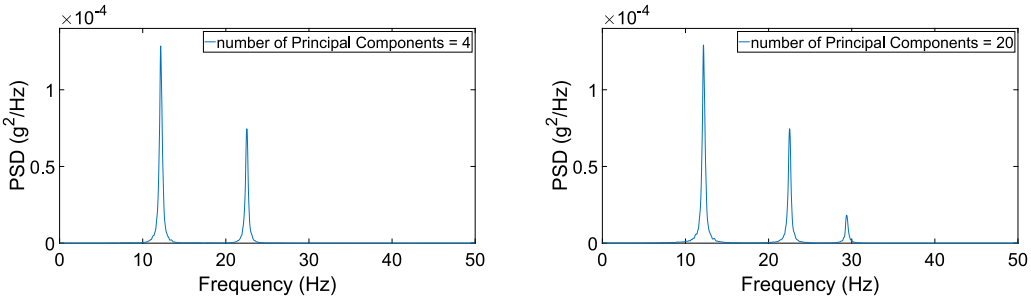

Fig. 4. Spectral density function of the reconstructed sensor in the frequency domain for the numbers 4 (left) and 20 (right) principal components.

obtained, as illustrated in Fig. 6. A 10% reduction in the stiffness of spring k_{11} leads to a change in the dynamic behavior of the system. For both excitation positions, the stiffness reduction results in the highest value obtained corresponding to mass m_1. This trend holds true for the subsequent damage positions, which can be consistently identified using the residual covariance.

In principle, the autoencoder with non-standardized time series is well suited for system identification and damage analysis. When evaluating the residuals of the autoencoder, advantages of the residual covariance, which is further only used as a damage position indicator, over the reconstruction error are clearly shown in Figs. 5 and 6. For practical application, an unmodified 10 min data set is learned and the natural frequencies are used to dimension the autoencoder, so there is easy transferability to other structures here. The decisive benefit of the autoencoder is the independence of the excitation position due to its computational structure; the information is compressed in the bottleneck dimension. Obviously, the excitation at mass m_1 only leads to the largest amplitudes at the mass m_1, but the reconstruction error is approximately the same (cf. 5), leading to a favorable baseline for damage localization. In particular, this is useful for tower structures that experience the largest amplitudes in the upper region.

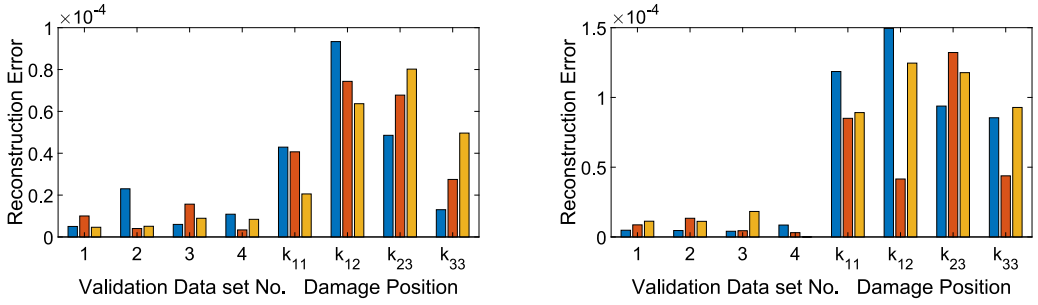

Fig. 5. Reconstruction errors as a damage position indicator for Gaussian distributed force at all masses (left) and at mass m_1 only (right).

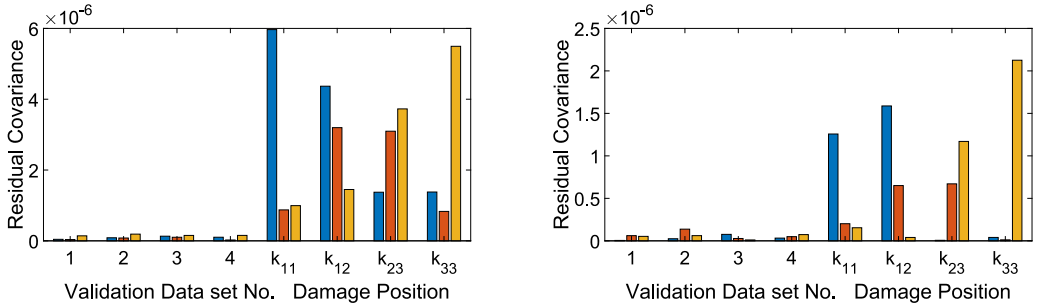

Fig. 6. Residual covariance as a damage position indicator for Gaussian distributed force at all masses (left) and at mass m_1 only (right).

Table 2
Modal parameters of the system identified from experimental data for healthy and damaged states.

Name	Position	B2-y	B3-y	B4-y	B5-y
Healthy	–	15.94 Hz	40.76 Hz	69.15 Hz	100.98 Hz
(A)	All struts at level 6	14.30 Hz	**34.88 Hz**	61.55 Hz	94.29 Hz
(B)	All struts at level 4	15.89 Hz	**38.92 Hz**	64.96 Hz	93.47 Hz
(C)	All struts at level 3	16.07 Hz	**37.08 Hz**	65.62 Hz	88.77 Hz
(D)	One strut at level 6	15.59 Hz	**40.79 Hz**	69.29 Hz	99.75 Hz
(E)	One strut at level 4	15.91 Hz	**40.46 Hz**	69.55 Hz	94.89 Hz
(F)	One strut at level 3	16.04 Hz	**40.91 Hz**	67.50 Hz	99.44 Hz

4. Experimental validation

For experimental validation, a lattice tower under ambient wind excitation is selected. Various positions within the structure can be deliberately damaged with varying degrees of severity. Section 4.1 presents the structure and data acquisition; additionally, the identification of natural frequencies based on 10 min data sets is carried out to gain further insights into the structural changes and to use these for the dimensioning of the autoencoder. The subsequently determined damage position indicators derived from the autoencoder are compared for varying damage positions (Section 4.2) in order to show robustness regarding excitation and influence of the environmental variability, which is further discussed in the last section (Section 4.3).

4.1. LUMO

LUMO is a test facility for SHM comprising a lattice tower exposed to realistic conditions and featuring multiple damage mechanisms [34]. The steel lattice mast is mounted on a concrete block foundation, which is situated on a meadow 20 km south of Hanover (Lower Saxony, Germany). A photograph of the test structure and a schematic figure of the measurement levels (ML) are given in Fig. 7. The facility is equipped with 18 uniaxial accelerometers positioned at ML1–ML9 and linked to a data acquisition system. A sensor recording the structural temperature is also employed. The mast features reversible damage locations (DAM) are installed on six levels DAM1-DAM6, three of which are used, as shown in the figure. At each possible damage level, three bracings were equipped with the damage mechanism, giving 18 different positions to introduce localized stiffness changes. Damage to LUMO can be realized by loosening the coupling nuts of an M10 threaded rod so that the corresponding bracing is severed (stiffness reduction). For DAM6, the installed damage mechanism is shown in Fig. 8.

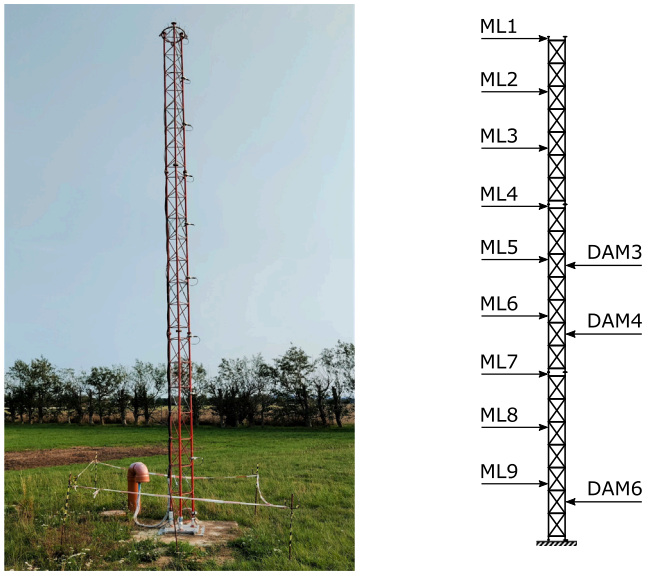

Fig. 7. Photograph of the lattice tower located near Hanover (left), and drawing of the levels equipped with acceleration sensors as well as the induced damage locations (DAM) (right) [34].

For further information, see [34]. Table 2 gives an overview of the different damage patterns and the corresponding average natural frequencies identified using covariance-driven stochastic subspace identification (SSI-COV) [13]. The y-direction was chosen here because the removal of one strut can be seen in the changed natural frequencies, while it cannot for the x-direction. While the first three damage patterns are symmetrical structural change, unscrewing only one connection results in asymmetrical damage.

As low frequencies have a lower sensitivity to structural changes, the fundamental frequency is chosen based on B3-y, and the sequence length is estimated using Eq. (3) to be 100 time steps long

$$l = 100 \geq 2\frac{1651.61}{34.88} = 94.70. \tag{11}$$

Consequently, the number of input neurons corresponding to the number of sensors multiplied by the estimated sequence length for each damage pattern results in 1800 input neurons. A suitable choice for the bottleneck dimension is determined using the scheme proposed in Section 2.2, which is based on the evaluation of the reconstruction error in the frequency domain. The resulting bottleneck dimensions are 543 (A), 641 (B), 664 (C), 692 (D), 700 (E), and 58 (F). It should be noted here that a new model must be trained for each damage instance because the repair led to a stiffening of the structure [34].

Difficulties in damage analysis of LUMO mainly result from excitation variation and dependence on temperature. The structural temperature is recorded, so 10 min data sets are classified according to their structural temperature, as shown in Table 3. In some cases, the number of data sets was increased by using a wider temperature range in order to have a sufficiently large database (at least 60 min) available. Moreover, the wind speed is estimated using the average variance of the lowest acceleration sensors in the tower, allowing a deviation of ten percent compared to the learning file. The effects of varying wind directions were not taken into account. A formula for estimating the maximum wind speed must be taken from [34] since the meteorological data was not recorded continuously.

4.2. Results

As mentioned earlier, the repair of the damage mechanisms is not perfect, i.e., the damage mechanisms are not perfectly reversible. For every damage pattern (A)–(F), a well-performing architecture for a neural network needs to be determined. A single 10 min data set per damage pattern, randomly chosen from the interval given in Table 3, is sufficient to train the model. This repetition, the training of a new autoencoder for each damage pattern, leads to a more meaningful evaluation of the real-life validation of the vibration-based damage localization approach. Under the assumption that the sensors closest to the damage show the maximum values, the corresponding residual covariances for the two accelerometers mounted at each measurement level are averaged. To better highlight the results, the residual covariances are normalized for each 10 min data set evaluated, and a threshold of 90% is defined. Sensors not close to the damaged location should not exceed this limit.

Fig. 8. Photograph of the concrete foundation (left), and the reversible damage mechanisms at level 6 (right) [34].

Table 3
Data selection from experimental data.

Name	T - learning μ (σ)	No. of data sets learning | testing	T - testing μ (σ)	Approx. max. wind speeds [34]
(A)	14.31 °C (0.0409)	1 | 10	13.89 °C (0.3032)	7.99–8.19 m/s
(B)	11.38 °C (0.1123)	1 | 9	11.17 °C (0.2598)	4.75–4.83 m/s
(C)	2.13 °C (0.0751)	1 | 10	1.67 °C (0.7100)	4.10–4.28 m/s
(D)	18.59 °C (0.2560)	1 | 8	18.77 °C (0.3704)	5.3–5.49 m/s
(E)	22.10 °C (0.7009)	1 | 6	24.66 °C (2.6125)	6.62–6.77 m/s
(F)	17.20 °C (0.0061)	1 | 7	16.69 °C (0.5226)	<0.5 m/s

Fig. 9 illustrates the normalized residual covariances evaluating 10 min data sets for damage pattern (A). The data represents the local stiffness changes mainly linked to the induced damage next to measurement level 9, or more precisely, damage level 6. Each bar of the measurement level represents a different evaluation of a 10 min data set. A gray bar is manually incorporated to highlight the sensors closest to the damage. To identify the removal of all struts at level 6, we can analyze the localization by comparing the residual covariance. The highest value is observed at measurement level 9, representing the geometrically lowest measurement level and slightly above the location where the first damage was induced. On average, the second highest residual covariance value is 0.36, corresponding to measurement level 8. The residual covariance values generally decrease as we move away from the induced damage. However, it is worth noting that measurement levels 1 and 6 deviate from the decreasing pattern observed at other distances from the damage.

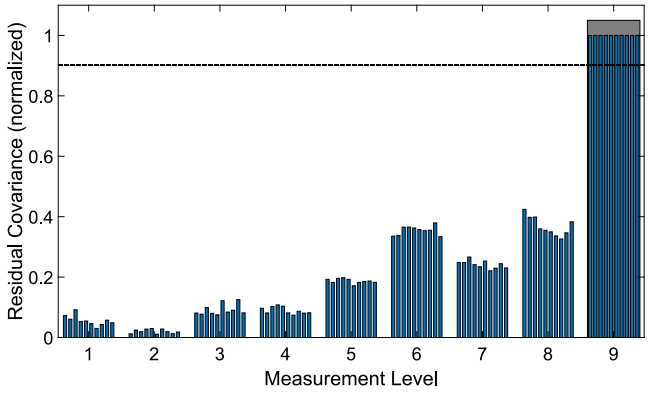

Fig. 9. Residual covariance for localization when removing all struts at damage level 6 (ML closest to damage in gray).

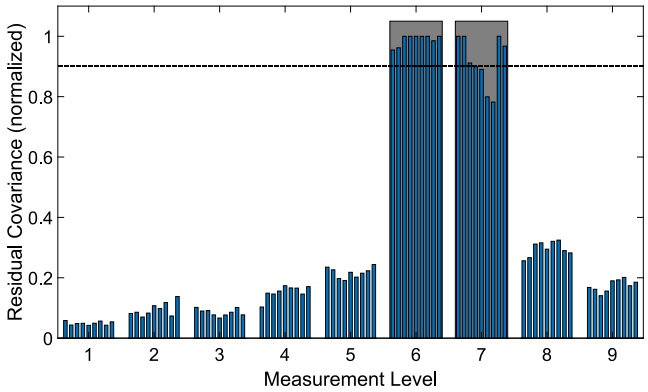

Fig. 10. Residual covariance for localization when removing all struts at damage level 4 (MLs closest to damage in gray).

The structural stiffness undergoes a change between measurement levels 6 and 7 in the case of damage pattern (B). The outcomes of the investigated method are visualized in Fig. 10. Consistent with previous observations, the local increase in residual covariance provides valuable insights for localization purposes. Predominantly, the values are correctly the highest at measurement level 6. Notably, the highest residual covariance value outside the gray area is 0.30, corresponding to measurement level 8. As the distance from the damage increases, the residual covariance values exhibit a clear decreasing trend. The smallest values of the damage identifier are at 0.05 at the top of the structure, which is also the measurement level furthest away from the damage.

The findings pertaining to damage pattern (C) are illustrated in Fig. 11. The figure specifically highlights the occurrence of the third structural change between measurement levels 5 and 6. Interestingly, despite the sensors at measurement level 5 being closer to the damage position, the values recorded at measurement level 6 are higher than

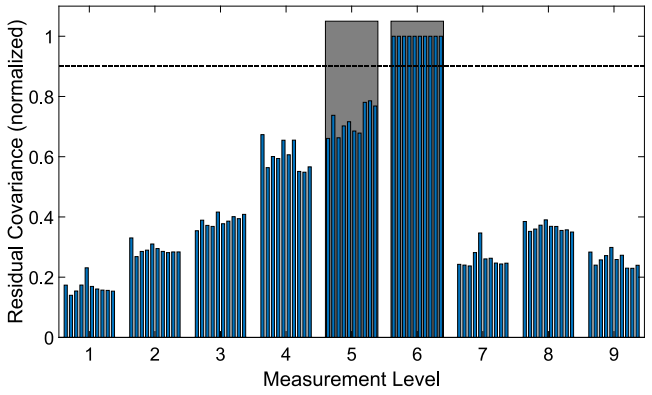

Fig. 11. Residual covariance for localization when removing all struts at damage level 3 (MLs closest to damage in gray).

those at measurement level 5. The lattice tower is fixed at the bottom, allowing for unconstrained vibration at the top. These boundary conditions might contribute to variations in the measured values, explaining the higher values at measurement level 6 compared to measurement level 5. Moreover, the highest value not in direct proximity to the damage is 0.60, which corresponds to measurement level 4. It is worth noting that measurement level 4 represents the third-closest position to the damaged location. As we move further away from the damage, the residual covariance values generally decrease. However, this trend does not hold true for all measurement levels; measurement level 8 deviates from this trend.

Fig. 12 presents the results obtained from evaluating the fourth induced structural change, namely damage pattern (D). In this case, only one damage mechanism was removed at damage level 6. The highest values observed in the evaluation are consistently found at measurement level 9. As mentioned before, this indicates that the residual effects of the damage are most prominent at this particular measurement level. For the first time, due to the low severity of the damage, values recorded at the other measurement levels are relatively close to 90%. Notably, measurement level 1 exhibits the second-highest average value, reaching 0.60. This suggests that even though it is not the measurement level with the highest values, it still experiences a significant impact from the structural change. In contrast to the previous symmetrical damage situation, the asymmetrical damage scenario does not show a decreasing trend with greater distance from the damage position.

Fig. 13 illustrates the results obtained from evaluating the penultimate induced structural change, specifically focusing on damage pattern (E). The removal of only one damage mechanism was performed at

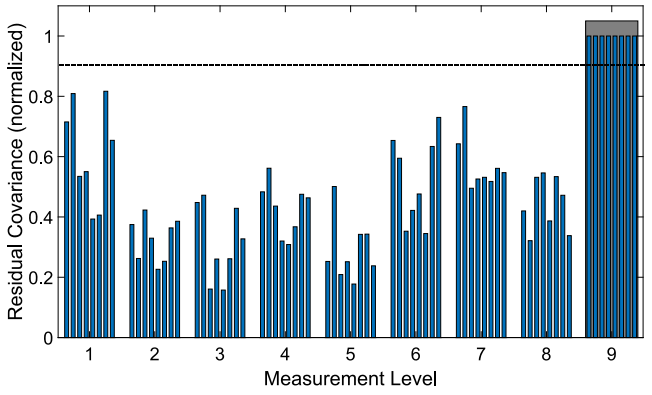

Fig. 12. Residual covariance for localization when removing one strut at damage level 6 (ML closest to damage in gray).

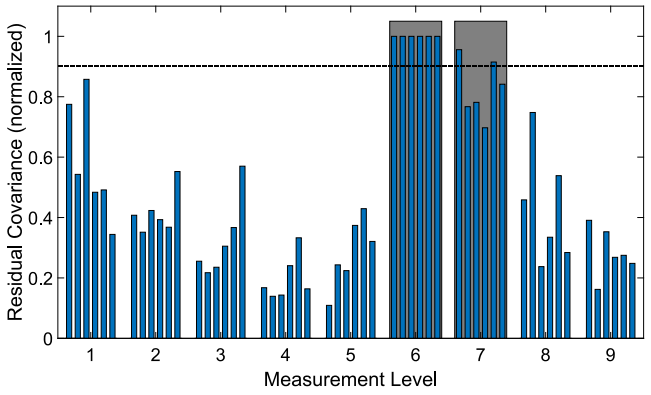

Fig. 13. Residual covariance for localization when removing one strut at damage level 4 (MLs closest to damage in gray).

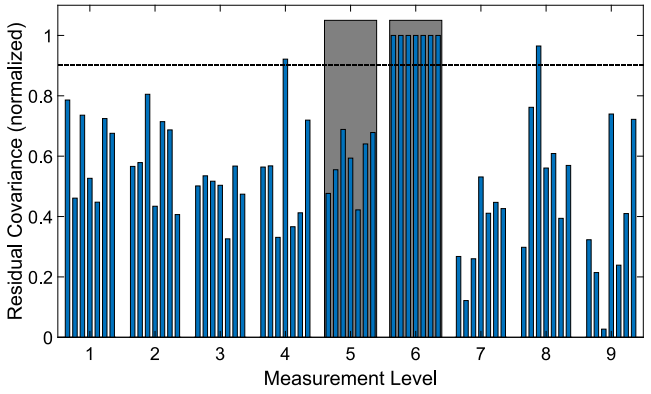

Fig. 14. Residual covariance for localization when removing one strut at damage level 3 (MLs closest to damage in gray).

damage level 4. It is noteworthy that for all the 10 min data sets utilized in the evaluation, successful localization of the damage was achieved. Consistent with the previous observation, measurement level 1 stands out with the third-highest values, averaging 0.58. The third evaluated 10 min data set shows a value of over 0.8 for measurement level 1, indicating a decreasing sensitivity towards the structural change regarding the asymmetrical damage scenario. Furthermore, no decreasing trend with increasing distance from the damage position is observed.

Fig. 14 illustrates the outcomes obtained from the evaluation of the most recent induced structural change, namely damage pattern (F). In the third asymmetrical damage scenario, a single damage mechanism was removed at damage level 3. The evaluation of all the utilized 10 min data sets consistently resulted in the highest obtained values at measurement level 6. This highlights the robustness and effectiveness of the employed methodology in accurately identifying the precise location of the structural change. Consistent with earlier observations regarding asymmetrical damage, measurement level 1 stands out with the third-highest values, exhibiting an average of 0.62 and the highest overall obtained value considering damage patterns (A) to (F). Moreover, at measurement levels 4 and 8, the threshold is exceeded.

4.3. Discussion

As the damage localization method has been only applied using non-standardized time series data, the advantages over choosing the spectrum of the time signal or the modal parameters of the structure have yet to be shown. Nevertheless, the reasons for the good results are clear: as little as possible was changed to increase the general applicability and the potential of the neural network to process unfiltered information. We have concluded that standardization has a

considerable influence on the quality of the results and was therefore not used in the proposed method. In particular, we consider the changes to the input time series to be critical, as the frequency space is changed and information is lost. Further, the dimensioning of the autoencoder becomes increasingly more difficult.

The investigations in Section 3 show that the proposed method is well suited to the task, as the damage position can be identified independently of the excitation position. Notably, four different damage positions were evaluated simultaneously. As described, the residual covariance (cf. Fig. 6) proves to be more potent than the reconstruction error (cf. Fig. 5) when evaluating the same autoencoders' residuals. The explanation for this was the additional consideration of the inputs, as discussed in Section 2.3.

For experimental validation, Figs. 9 to 11 show that the position of the damage can be consistently identified. Interestingly, the damage position indicators become smaller with increasing distance from the induced structural change, implying that a lower sensor resolution would still have been sufficient. Damage relatively far down could be better localized. For the minor structural changes, the damage localization is consistently successful but not so precise, as can be seen in Figs. 12 to 14, for which the reasons are manifold. Due to summer's lower wind speeds, the eigenfrequencies were less excited. The time between induced damage instances was chosen to be shorter, leading to a smaller database for learning. Considering the evaluation method, the damage position indicator was averaged for each measurement level for better comparability and to show robustness, even though the damage was only induced in the y-direction. It should also be noted that the loosening of a strut leads to asymmetrical damage and, therefore, to a more significant change in the torsional modes, which is not favorable for damage localization and led to large values at the top of the structure.

In comparison to different data-driven approaches such as PALS-tuned Kalman filters [13] and finite impulse response filters [16] working on LUMO, we have successfully shown that it is possible to localize minor damage-induced structural changes. The damage localization method succeeds especially due to the autoencoder's ability to consistently determine the correct damage position. Regarding the autoencoder's structure, the sequences are encoded in the bottleneck, as already mentioned in Section 3.2, which results in signals with different amplitudes (e.g., from tower structures) having similar reconstruction errors when evaluating the healthy state. Accordingly, one has an excellent baseline, robust against varying excitation position, to monitor the position of the structural changes.

5. Conclusion

In this paper, we investigated an autoencoder with non-standardized time series data for unsupervised damage localization in vibration-based SHM. To this end, we established an approach to effectively use raw acceleration signals as the inputs of an autoencoder for system identification. To make this approach generally applicable, an automated solution is provided to operate the neural architecture search. As part of this, the bottleneck dimension is estimated using the PCA by evaluating the frequency domain of the reconstructed signals. As an extension to the model, we assessed the covariance of the inputs and the residuals of the network to improve the proposed method's performance. Examining the simulation results, the covariance proved to be more robust and sensitive towards the damage position than the reconstruction error. It has also been shown that the autoencoder is robust towards different excitation positions, which suggests that the model mainly learns the system properties. Experimental validation was further conducted, in which the autoencoder performed exceptionally well. Classifying the 10 min data sets according to wind speed and structure temperature was sufficient. As the distance from the damage increases, the residual-based damage position indicators exhibit a decreasing trend for symmetrical damage. Minor structural changes can also be localized consistently; probably due to torsional eigenmodes a gradual decline in values as we move further away from the damaged area was not found, which is a drawback of the proposed method. In addition, the residuals of the autoencoder cannot be physically interpreted and are therefore more susceptible to incorrect decision-making processes. In summary, applying autoencoders with time series data using the covariance of the inputs and the residuals promises to be a potent tool for unsupervised damage localization.

For future work, trying to localize the damage under varying environmental conditions using autoencoders is a problem to tackle. The number of learning files can be increased to cover a larger temperature range. For further development, more complex failure modes involving the interaction of multiple factors or components within a system should be examined. A comparative study should be conducted to investigate different characteristics and advantages of variations of the autoencoder, such as a variational or convolutional autoencoder. The covariance-based residual analysis is motivated by the non-trivial interpretability of neural networks. Nevertheless, the damage-sensitive feature can also be applied to different models' residuals. The approach was deliberately kept general to allow easy transferability of the application to other systems, such as wind turbines. Further, data-based system identification could be transferred to nonlinear systems (e.g., rotor blades).

CRediT authorship contribution statement

Niklas Römgens: Investigation, Methodology, Software, Supervision, Writing – original draft, Writing – review & editing. **Abderrahim Abbassi:** Software. **Clemens Jonscher:** Methodology, Writing – review & editing. **Tanja Grießmann:** Funding acquisition, Writing – review & editing. **Raimund Rolfes:** Funding acquisition, Writing – review & editing.

Declaration of competing interest

The authors declare that they have no known competing financial interests or personal relationships that could have appeared to influence the work reported in this paper.

Data availability

Data will be made available on request.

Declaration of Generative AI and AI-assisted technologies in the writing process

During the preparation of this work, the authors used ChatGPT in order to improve the language. After using this tool, the authors reviewed and edited the content as needed and take full responsibility for the content of the publication.

Acknowledgments

The authors gratefully acknowledge the financial support provided by the Federal Ministry for Economic Affairs and Climate Action of the Federal Republic of Germany within the framework of the collaborative research project Grout-WATCH (FKZ 03SX505B) and SMARTower (FKZ 03EE2041C). All authors approved the version of the manuscript to be published.

References

[1] Rastin Z, Amiri G, Darvishan E. Unsupervised structural damage detection technique based on a deep convolutional autoencoder. Shock Vib 2021;1–11.

[2] Rytter A. Vibrational based inspection of civil engineering structures. Aalborg University, Aalborg: Department of Building Technology and Structural Engineering; 1993.

[3] Farrar C, Worden K. Structural health monitoring: A machine learning perspective. Chichester: Wiley; 2012.

[4] Shokrani Y, Dertimanis V, Chatzi E, Savoia M. On the use of mode shape curvatures for damage localization under varying environmental conditions. Struct Control Health Monit 2018;25(4):e2132.

[5] Ou Y, Dertimanis V, Chatzi E. Operational damage localization of wind turbine blades. In: Conte J, Astroza R, Benzoni G, Feltrin G, Loh K, Moaveni B, editors. Experimental vibration analysis for civil structures. Springer International Publishing 2018; 2018, p. 261–72. http://dx.doi.org/10.1007/978-3-319-67443-8_22.

[6] Fan W, Qiao P. Vibration-based damage identification methods: A review and comparative study. Struct Health Monit 2011;10(1):83–111.

[7] Avendano-Valencia L, Chatzi E, Tcherniak D. Gaussian process models for mitigation of operational variability in the structural health monitoring of wind turbines. Mech Syst Signal Process 2020;142:106686.

[8] Mottershead J, Friswell M. Model updating in structural dynamics: A survey. J Sound Vib 1993;167(2):347–75.

[9] Simeon E, Roeck GDe, Lombaert G. Dealing with uncertainty in model updating for damage assessment: A review. Mech Syst Signal Process 2015;56:123–49.

[10] Bruns M, Hofmeister B, Hübler C, Rolfes R. Damage localization via model updating using a damage distribution function. Struct Health Monit 2019;142:909–17.

[11] Bruns M, Hofmeister B, Grießmann T, Rolfes R. Comparative study of parameterizations for damage localization with finite element model updating. In: Beer M, Zio E, editors. Proceedings of the 29th European safety and reliability conference. 2019, p. 1125–32. http://dx.doi.org/10.3850/978-981-11-2724-3_0713-cd.

[12] Wolniak M, Hofmeister B, Jonscher C, Fankhänel M, Loose A, Hübler C, Rolfes R. Validation of an FE model updating procedure for damage assessment using a modular laboratory experiment with a reversible damage mechanism. J Civ Struct Health Monit 2023;1–22.

[13] Wernitz S. Damage localization in data-driven vibration-based structural health monitoring using linear quadratic estimation theory. Hannover: Gottfried Wilhelm Leibniz Universität; 2023.

[14] Mosavi A, Dickey D, Seracino R, Rizkalla S. Identifying damage locations under ambient vibrations utilizing vector autoregressive models and mahalanobis distances. Mech Syst Signal Process 2012;26:254–67.

[15] Chesné S, Deraemaeker A. Damage localization using transmissibility functions: A critical review. Mech Syst Signal Process 2013;38(2):569–84.

[16] B. Hofmeister. Vibration-based damage localisation: impulse response identification and model updating methods. Hannover: Gottfried Wilhelm Leibniz Universität; 2023.

[17] Alves V, Cury A. An automated vibration-based structural damage localization strategy using filter-type feature selection. Mech Syst Signal Process 2023;190:110145.

[18] Anaissi A, Zandavi SM, Suleiman B, Naji M, Braytee A. Multi-objective autoencoder for fault detection and diagnosis in higher-order data. In: 2019 international joint conference on neural networks. IEEE; p. 1–8. http://dx.doi.org/10.1109/IJCNN.2019.8852305.

[19] Ma X, Lin Y, Ma H. Structural damage identification based on unsupervised feature-extraction via variational Auto-encoder. Measurement 2020;160:107811.

[20] Zhang Y, Xie X, Li H, Zhou B. An unsupervised tunnel damage identification method based on convolutional variational auto-encoder and wavelet packet analysis. Sensors 2022 2022;22(6):2412.

[21] Römgens N, Abbassi A, Jonscher C, Grießmann T, Rolfes R. Unsupervised damage localization using autoencoders with time-series data. In: 10th international conference on experimental vibration analysis for civil engineering structures. 2023, http://dx.doi.org/10.1007/978-3-031-39117-0{_}52.

[22] Hong C, Yu J, Wan J, Tao D, Wang M. Multimodal deep autoencoder for human pose recovery. IEEE Trans Image Process 2015;24(12):5659–70.

[23] Germain M, Gregor K, Murray I, Larochelle H. Made: Masked autoencoder for distribution estimation. In: International conference on machine learning. 2015, p. 881–9. http://dx.doi.org/10.48550/arXiv.1502.03509.

[24] An J, Cho S. Variational autoencoder based anomaly detection using reconstruction probability. Special Lecture on IE 2015;2:1–18.

[25] Pathirage C, Li J, Li L, Hao H, Liu W, Ni P. Structural damage identification based on autoencoder neural networks and deep learning. Eng Struct 2018;172:13–28.

[26] Nikolopoulos S, Kalogeris I, Papadopoulos V. Machine learning accelerated transient analysis of stochastic nonlinear structures. Eng Struct 2022;257:114020.

[27] Abbassi A, Römgens N, Tritschel F, Penner N, Rolfes R. Evaluation of machine learning techniques for structural health monitoring using ultrasonic guided waves under varying temperature conditions. Struct Health Monit 2023;22(2):1308–25.

[28] Kingma D, Ba J. Adam: A method for stochastic optimization. 2014, arXiv preprint arXiv:1412.6980.

[29] Hsu T-Y, Valentino A, Liseikin A, Liseikin A, Krechetov D, Chen C-C, et al. Continuous structural health monitoring of the Sayano-Shushenskaya Dam using off-site seismic station data accounting for environmental effects. Meas Sci Technol 2019;31(1):015801.

[30] Anaissi A, Zandavi S, Suleiman B, Naji M, Braytee A. Multi-objective variational autoencoder: An application for smart infrastructure maintenance. Appl Intell 2023;53(10):12047–62.

[31] Sarwar M, Cantero D. Deep autoencoder architecture for bridge damage assessment using responses from several vehicles. Eng Struct 2021;246:113064.

[32] Boquet G, Macias E, Morell A, Serrano J, Vicario J. Theoretical tuning of the autoencoder bottleneck layer dimension: A mutual information-based algorithm. In: 28th European signal processing conference. 2020, p. 1512–6. http://dx.doi.org/10.23919/Eusipco47968.2020.9287226.

[33] Penner N. Monitoring ambient angeregter baudynamischer systeme durch mehrschichtige perzeptren. Institut für Statik und Dynamik, Hannover; 2022.

[34] Wernitz S, Hofmeister B, Jonscher C, mann T, Rolfes R. A new open-database benchmark structure for vibration-based structural health monitoring. Struct Control Health Monit 2022;29(11):e3077.